

Ionized Gas in the Irr Galaxy IC 10: The Emission Spectrum and Ionization Sources

V.P. Arkhipova ¹, O.V. Egorov ¹, T.A. Lozinskaya ¹, A.V. Moiseev ²

ABSTRACT

We present the results of observations of the Irr galaxy IC 10 at the 6-m SAO telescope with the panoramic Multi-Pupil Fiber Spectrograph (MPFS). Based on the results of these observations and our long-slit spectroscopy performed previously, we have investigated the ionized-gas emission spectrum in the region of intense star formation and refined the gas metallicity estimates. We show that the “diagnostic diagrams” constructed from our observations agree best with the new improved ionization models by Martín-Manjón et al. Using these models, we have determined the electron density and gas ionization parameter and ionizing-cluster characteristics, the age and mass, from the spectra of the investigated HII regions. The cluster age and mass are shown to be within the ranges 2.5 – 5 Myr and $(0.2 - 1) \times 10^5 M_{\odot}$, respectively.

Subject headings: dwarf Irr galaxies, IC 10, star-forming regions, spectra, ages, photoionization models of HII regions.

INTRODUCTION

Studies of Local Group irregular galaxies open optimal possibilities for investigating the structure, kinematics, and chemical composition of the gaseous medium and their changes not only during the evolution of Irr galaxies but, according to present views, also during the evolution of massive galaxies. The topicality of detailed studies of the gas emission spectrum and ionization conditions in the nearest dwarf Irr galaxy IC 10 is determined by a number of its peculiarities. The anomalously large number of Wolf–Rayet (WR) stars in IC 10 arouses the greatest interest. The space density of WR stars here is highest among the dwarf galaxies, comparable to that in massive spiral galaxies (Massey et al. 1992; Richer et al. 2001; Massey and Holmes 2002; Crowther et al. 2003; Vacca et al. 2007). The stellar population of IC 10 is indicative of both a recent starburst ($t=3 - 10$ Myr) and an older starburst ($t > 350$ Myr)

(Hunter 2001; Zucker 2002; Massey et al. 2007; Vacca et al. 2007; and references therein). The high $H\alpha$ and infrared luminosities and the anomalously large number of WR stars in IC 10 suggest that the last starburst was short but it affected the bulk of the galaxy.

The gas and stellar compositions of the galaxy have been well studied (and are being intensively studied). Not coincidentally, it is for IC 10 that Yin et al. (2010) performed detailed model calculations of the evolution of the chemical composition in an Irr galaxy for various star formation and galactic wind regimes.

In this paper, we continue our studies of the gas emission spectrum in the dwarf Irr starburst galaxy IC 10 begun by Lozinskaya et al. (2009). The main objective of the first paper was to determine the gas metallicity in about twenty HII regions and in the synchrotron superbubble from our observations of the galaxy at the 6-m SAO telescope with the SCORPIO focal reducer in the long-slit mode (the chemical composition of only the three brightest nebulae in the galaxy was known previously; see Lozinskaya et al. (2009) and references therein.) The paper by Magrini and Gonçalves (2009), who determined the chemical

¹Sternberg Astronomical Institute, Universitetskii pr. 13, Moscow, 119992 Russia, E-mail: vera@sai.msu.ru

²Special Astrophysical Observatory, Russian Academy of Sciences, Nizhny Arkhyz, Karachai-Cherkessian Republic, 357147 Russia

composition of many HII regions and planetary nebulae in IC 10, appeared in the same year.

The main goal of our new paper is to analyze the emission spectrum and gas ionization state by the galaxy's stellar population. This study is based on our observations performed at the 6-m SAO telescope with the panoramic Multi-Pupil Fiber Spectrograph (MPFS). Since these observations are interpreted in terms of the new improved ionization models by Martín-Manjón et al. (2009) and are compared with the new computations by Levesque et al. (2009), we deemed it appropriate to also reconsider the results of our long-slit spectroscopy presented in Lozinskaya et al. (2009) in terms of these models. The data on the stellar population of IC 10 were also updated significantly over the year: two papers devoted to the search for star clusters in the galaxy appeared simultaneously (Tikhonov and Galazutdinova 2009; Sharina et al. 2009). Previously, Hunter (2001) identified clusters only in the region of intense current star formation and in its immediate neighborhood; in the mentioned new papers, the investigated galactic regions were extended and the number of clusters increased significantly.

The most interesting region that we studied in greatest detail is the bright complex of ionized gas in the southeastern section of the galaxy, in which the last starburst episode most likely occurred in IC 10 (Vacca et al. 2007). Here, there are the densest HI cloud, a molecular CO cloud, and a complex of emission nebulae about 300–400 pc in size, including two bright shell nebulae, HL111 and HL106 (according to the catalog by Hodge and Lee (1990)), as well as the youngest star clusters and ten WR stars (Leroy et al. 2006; Wilcots and Miller 1998; Gil de Paz et al. 2003; Lozinskaya et al. 2009; Egorov et al. 2010; and references therein). The size of the shell HL111 determined by its three arc parts HL111c, HL111d, and HL111e is about $10''$ or 39 pc. An object previously identified as the WR star M24 (in what follows, the WR stars from the lists by Royer et al. (2001) and Massey and Holmes (2002) are denoted by the letters R and M, respectively) is located in the nebula HL111c, which represents the brightest part of the shell. According to present views (see Vacca et al. 2007), M24 is a close group of stars that consists of at least six blue stars; four of them are possible WR candidates.

The galaxy's H α and [SII] images reveal fainter multiple shells and supershells with sizes from 50 pc to 800–1000 pc outside this brightest complex (Zucker 2000; Wilcots and Miller 1998; Gil de Paz et al. 2003; Leroy et al. 2006; Chyzy et al. 2003; Lozinskaya et al. 2008). Some of the MPFS fields and long-slit spectrograms are localized in these faint regions.

A unique object, the so-called synchrotron superbubble, is adjacent to the central bright star formation complex on the south. Lozinskaya and Moiseev (2007) were the first to explain the formation of the synchrotron superbubble by a hypernova explosion; previously, its formation was associated with multiple explosions of about ten supernovae (Yang and Skillman 1993; Bullejos and Rozado 2002; Rosado et al. 2002; Thurov and Wilcots 2005).

In the succeeding sections, we describe our observations, present and discuss our results, and, in conclusion, summarize our main conclusions.

All radial velocities here are heliocentric; the distance to the galaxy is taken to be 800 kpc (the angular scale is $\simeq 3.9$ pc $''$) (Sanna et al. 2009; Tikhonov and Galazutdinova 2010).

OBSERVATIONS AND DATA REDUCTION

MPFS Observations

The selected galactic regions were observed with the panoramic Multi-Pupil Fiber Spectrograph (MPFS) mounted at the prime focus of the 6-m telescope (see Afanasiev et al. (2001) and the web site¹). The detector was an EEV 42–20 2048 \times 2048-pixel CCD array. The spectrograph can simultaneously record the spectra from 256 spatial elements (spaxels) (in the shape of square lenses) that constitute a 16 \times 16-spaxel array in the plane of the sky. The angular size of a single spaxel is $1''$.

In this paper, we use the spectra of five fields with a resolution of about 6.5 Å in the wavelength range 3990–6940 Å taken for IC 10 (in the sixth field around the WR star M23, the emission turned out to be very weak.) The localization of the MPFS fields in the galactic image is shown in

¹<http://www.sao.ru/hq/lsvfo/devices.html>

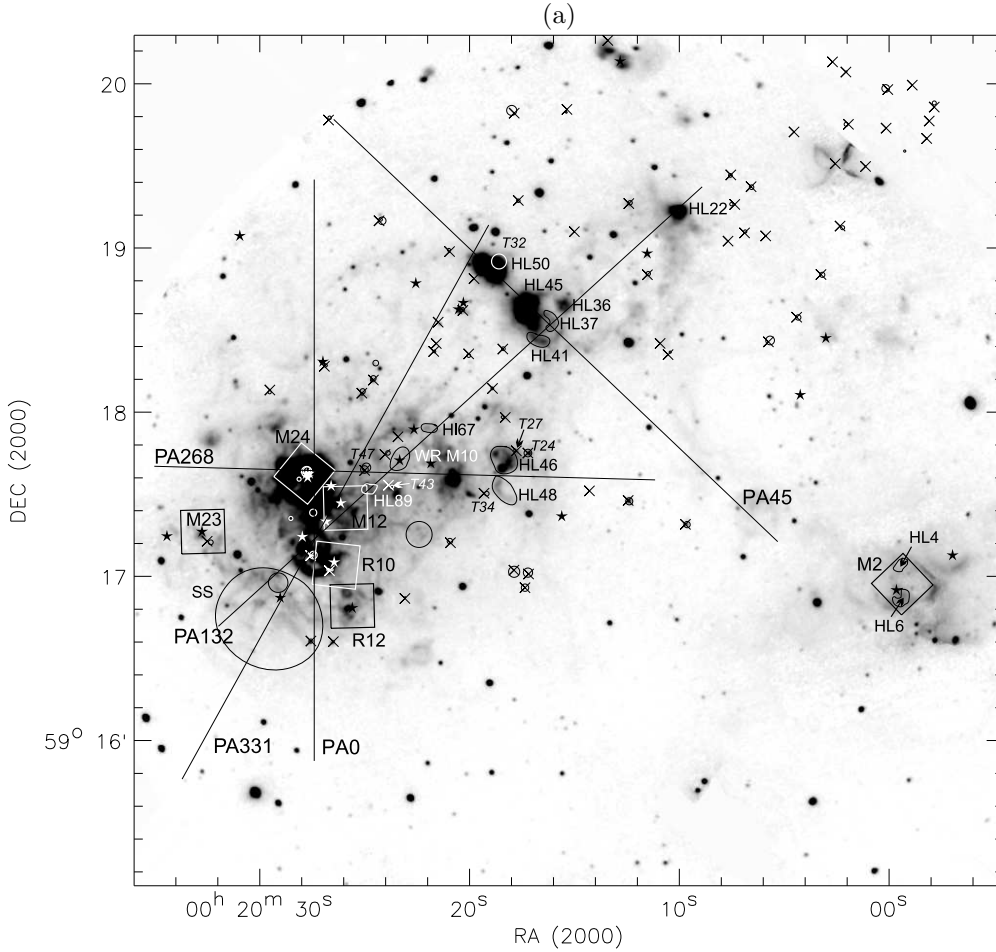


Fig. 1.— Localization of five long-slit spectrograms and six MPFS fields in the $H\alpha$ image of IC 10: (a) the entire galaxy and (b) the brightest region of current star formation. The MPFS fields are designated according to their central WR star; the long-slit spectrograms, as in Lozinskaya et al. (2009), are designated according to their position angle. The asterisks mark the spectroscopically confirmed WR stars from the lists by Royer et al. (2001) and Massey and Holmes (2002). The circles indicate the star clusters from the lists by Hunter (2001) and Tikhonov and Galazutdinova (2010); the crosses indicate the centers of the clusters from the list by Sharina et al. (2009). The clusters used in the text are denoted by the letter T and the number from the list by Tikhonov and Galazutdinova (2010). Also shown are the HII regions over which the lines presented in Table 3 were integrated.

Fig. 1; the fields are designated according to the central WR star.

We reduced the observations using the software developed at the SFVO laboratory of the SAO, the Russian Academy of Sciences, and running in the IDL environment. The spectra of the stars BD+75^d325 and G191-B2B observed immediately after the object were used for energy calibration. The result of this reduction is a “data cube” in

which a 2048-pixel spectrum corresponds to each spaxel of the $16'' \times 16''$ image.

Long-Slit Spectroscopy

We also used the observations of IC 10 with the SCORPIO instrument (for a description, see Afanasiev and Moiseev 2005) operating in the long-slit mode. The observations were performed with a slit about $6''$ in length and $1''$ in

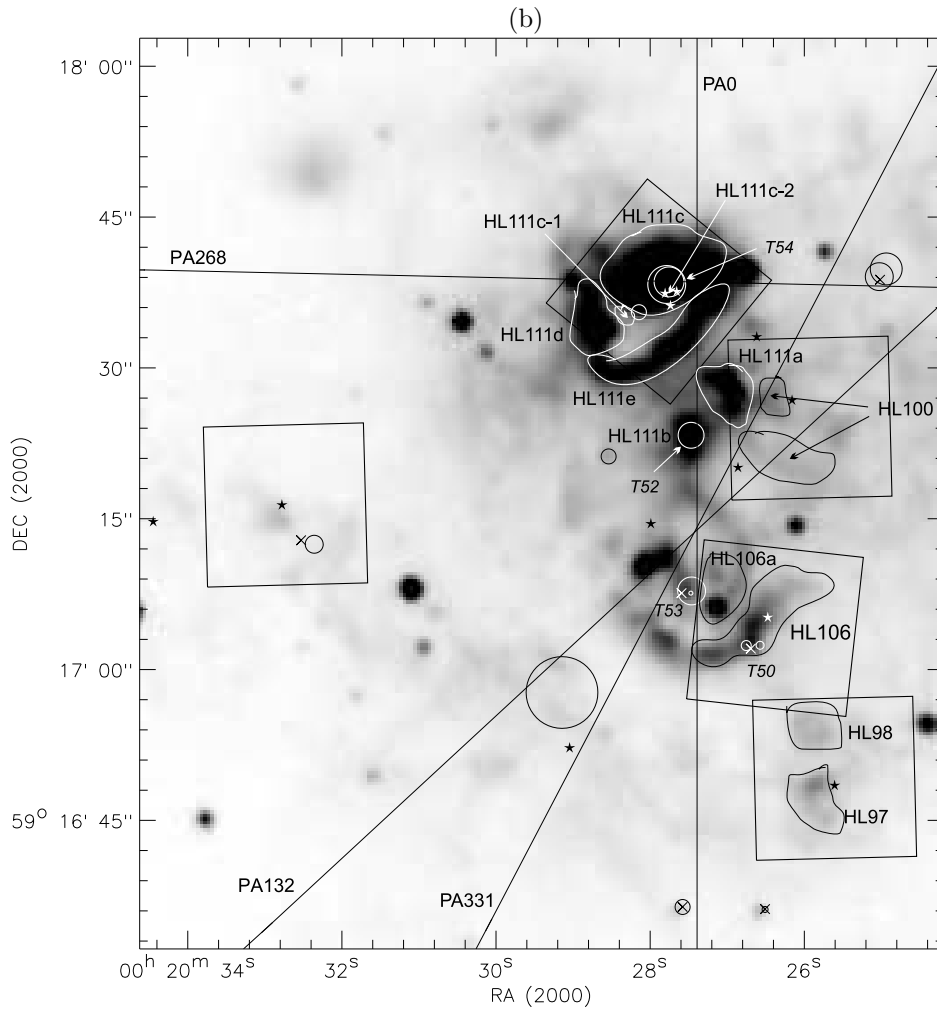


Fig. 1.— (Contd.)

width; the scale along the slit was $0.36''$ per pixel. The technique of these observations and the results obtained are described in detail in Lozinskaya et al. (2009).

For five slit positions designated in accordance with their position angles as PA0, PA45, PA132, PA268, and PA331, we took spectra with a resolution from 2.5 to 9 Å. The localization of the spectrograms is shown in Fig. 1.

To increase the signal-to-noise ratio for faint emission regions, we performed an averaging over individual nebulae when processing the spectrograms; the region of integration was from 2 to $20''$ in size.

The ranges of errors given below in the tables and figures correspond to 3σ .

A log of MPFS and SCORPIO long-slit observations is presented in Table 1. Its columns give: (1)—MPFS field designated according to the central WR star or spectrogram designated according to its position angle; (2)—date of observations; (3)—spectral range; (4)—spectral resolution; (5)—total exposure time; (6)—“seeing”.

Here, we also partly use the observational data obtained with SCORPIO in the mode of a Fabry–Perot interferometer in the $H\alpha$ and [SII] lines presented previously in Egorov et al. (2010).

RESULTS OF OBSERVATIONS

The localization of the six MPFS fields and five long-slit spectrograms that were analyzed in detail in Lozinskaya et al. (2009) and partially used in this paper in the $H\alpha$ image of the galaxy is shown in Fig. 1. The spectroscopically confirmed WR stars from the lists by Royer et al. (2001) and Massey and Holmes (2002) as well as the star clusters from the lists by Hunter (2001), Tikhonov and Galazutdinov (2010), and Sharina et al. (2010) are labeled in the figure.

In the list of cluster coordinates presented by Tikhonov and Galazutdinova (2010) and in the coordinates of the M24 group of stars in Vacca et al. (2007), we revealed a shift by about $2''.4$ related to the referencing of the coordinate system of HST observations. After an appropriate refinement of the coordinates (Vacca, private communication; Galazutdinova, private communication), the localizations of the common clusters in the three mentioned lists in Fig. 1 agree well in

most cases (the refined coordinates are given in the updated version of the paper by Tikhonov and Galazutdinova (2009): arXiv:1002.2046v1 [astro-ph.GA])

For the convenience of identification, the HII regions from the list by Hodge and Lee (1990) mentioned in the text and the synchrotron superbubble (denoted by SS in Fig. 1a) are also labeled in Figs. 1a and 1b. The two separate areas of the nebula HL111c in Fig. 1b and in Table 3 (see below) are designated as HL111c-1 and HL111c-2.

The observations of several galactic regions were performed both with the MPFS and long-slit spectrograph (see Fig. 1), which allows the actual accuracy of our measurements to be estimated. For this purpose, we determined the integrated relative intensities of several lines for the regions falling into the spectrograph slit and cut out the same regions in the corresponding MPFS field. Table 2 gives the relative line intensities in the same region measured from our long-slit spectrograms and MPFS observations. As we see, the agreement is good everywhere, within the error limits.

Previously (Lozinskaya et al. 2009), we made sure that the measurements made from two long-slit spectra at the points of their intersection are also in good agreement, given the difference between the regions of integration of the fluxes for different slit orientations.

The results of our processing of the MPFS spectra are presented in Table 3. Its columns give: (1)—MPFS field used and name of the HII region or its part over which the line flux was integrated; (2), (3), and (4) — integrated relative line intensities $I([\text{OIII}]\lambda 4959, 5007)/I(H\beta)$, $I([\text{SII}]\lambda 6717, 31)/I(H\alpha)$, and $I([\text{NII}]\lambda 6584)/I(H\alpha)$, respectively. The regions over which the integration was performed are shown in Figs. 1a and 1b; the two parts of the bright nebula HL111c are marked by the indices 1 and 2.

The relative line intensities averaged over the long-slit spectroscopic observations of the investigated nebulae are listed in Table 3 from Lozinskaya et al. (2009).

As an example, Fig 2 shows the distribution maps of relative line intensities: $I([\text{SII}]\lambda 6717 + 6731\text{Å})/I(H\alpha)$, $I([\text{NII}]\lambda 6584\text{Å})/I(H\alpha)$, and $I([\text{OIII}]\lambda 5007 + 4959\text{Å})/I(H\beta)$ for the MPFS field

Table 1: Log of observations

MPFS field/spectrum (PA)	Date	Range $\Delta\lambda$, Å	$\delta\lambda$, Å	T_{exp} , s	seeing
MPFS M24	Aug. 8/9, 2004	3990–6940	6.5	2700	1.7–2.0
MPFS R10	Aug. 8/9, 2004	3990–6940	6.5	1800	1.4
MPFS M12	Sep. 28/29, 2005	3990–6940	6.5	3600	2.0
MPFS R12	Sep. 28/29, 2005	3990–6940	6.5	3600	2.0
MPFS M2	Aug. 8/9, 2004	3990–6940	6.5	1200	1.5
MPFS M23	Sep. 28/29, 2005	3990–6940	6.5	2400	2.5
PA0	Aug. 17/18, 2006	3620–5370	5	6000	2.5
PA0	Sep. 2/3, 2008	5650–7340	5	3600	2.1
PA132	Aug. 17/18, 2006	3620–5370	5	4800	1.4
PA132	Aug. 18/19 2006	5650–7340	5	3600	1.4
PA268	Feb. 14/15, 2007	6060–7060	2.5	1200	1.4
PA268	Jan. 15/16, 2008	3620–5370	5	4800	1.5
PA45	Oct. 29/30, 2008	3650–7350	9	3600	1.0
PA331	Oct. 28/29, 2008	3650–7350	9	6000	0.9

Table 2: Relative line intensities in the regions of intersection between the spectrograph slits and MPFS fields

MPFS and spectrum	$\log(I([\text{OIII}]4959,5007)/I(\text{H}\beta))$	$\log(I([\text{SII}]6717,31)/I(\text{H}\alpha))$	$\log(I([\text{NII}]6584)/I(\text{H}\alpha))$
M24	0.69 ± 0.02	-0.97 ± 0.07	-1.31 ± 0.05
PA268	0.66 ± 0.02	-0.97 ± 0.02	-1.33 ± 0.02
M24	0.70 ± 0.02	-0.98 ± 0.07	-1.27 ± 0.04
PA0	0.67 ± 0.03	-0.86 ± 0.02	-1.32 ± 0.02
M12	0.47 ± 0.08	-0.32 ± 0.09	-0.84 ± 0.08
PA331	0.45 ± 0.07	-0.42 ± 0.02	-1.00 ± 0.05
M12	0.41 ± 0.08	-0.21 ± 0.07	-0.84 ± 0.09
PA132	0.34 ± 0.09	-0.18 ± 0.02	-0.75 ± 0.04
R10	0.43 ± 0.13	-0.42 ± 0.09	-0.93 ± 0.05
PA0	0.58 ± 0.11	-0.57 ± 0.05	-0.93 ± 0.03

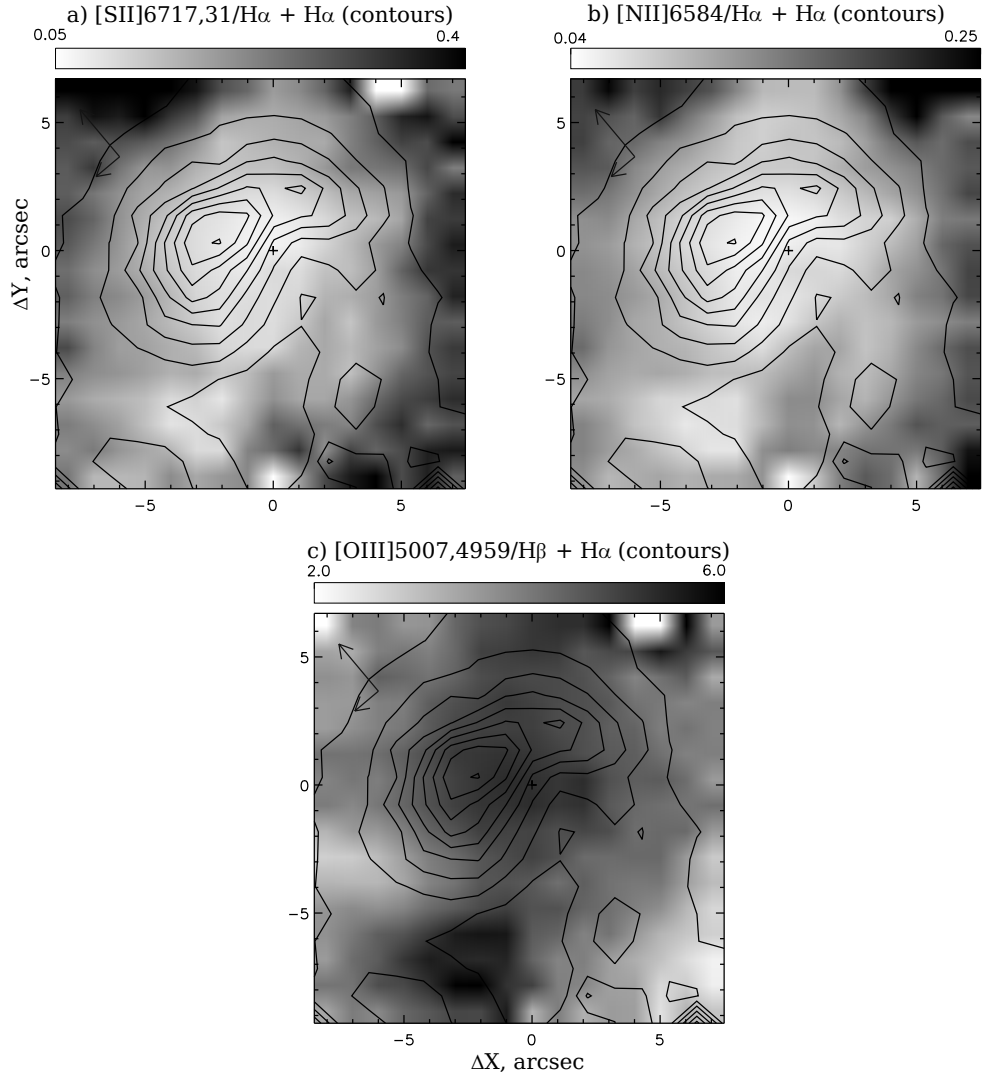


Fig. 2.— Distribution maps of relative line intensities: $I([\text{SII}]\lambda 6717 + 6731\text{\AA})/I(\text{H}\alpha)$ (a), $I([\text{NII}]\lambda 6584\text{\AA})/I(\text{H}\alpha)$ (b), and $I([\text{OIII}]\lambda 5007+4959\text{\AA})/I(\text{H}\beta)$ (c) for the MPFS field M24 (the region of the shell nebula HL111). The arrows in the upper left corner of the panels indicate the direction northward and eastward. The contours give the H α intensity.

Table 3: Relative line intensities from our MPFS observations

MPFS field and HII region	$I([\text{OIII}]4959,5007)/I(\text{H}\beta)$	$I([\text{SII}]6717,31)/I(\text{H}\alpha)$	$I([\text{NII}]6584)/I(\text{H}\alpha)$
M24 HL111c	4.74 ± 0.39	0.123 ± 0.038	0.058 ± 0.015
M24 HL111c-1	5.13 ± 0.44	0.131 ± 0.027	0.058 ± 0.011
M24 HL111c-2	5.32 ± 0.14	0.087 ± 0.009	0.063 ± 0.025
M24 HL111d	4.91 ± 0.62	0.156 ± 0.036	0.066 ± 0.016
M24 HL111e	3.98 ± 0.40	0.212 ± 0.063	0.083 ± 0.015
M12 HL100	1.93 ± 0.57	0.66 ± 0.14	0.162 ± 0.022
M12 HL111a	4.00 ± 1.50	0.38 ± 0.09	0.123 ± 0.023
R10 HL106	2.49 ± 0.73	0.39 ± 0.09	0.129 ± 0.004
R10 HL106a	2.89 ± 0.69	0.25 ± 0.04	0.102 ± 0.018
R12 HL97	5.8 ± 2.4	0.52 ± 0.12	0.153 ± 0.044
R12 HL98	3.4 ± 1.2	0.75 ± 0.25	0.165 ± 0.033
M2 HL4	4.6 ± 3.6	0.73 ± 0.22	0.162 ± 0.128
M2 HL6	8.4 ± 5.8	0.40 ± 0.18	0.117 ± 0.046

M24. The contours indicate the $\text{H}\alpha$ intensity.

DISCUSSION

Below, we compare the results of our observations of the emission spectrum for HII regions of IC 10 with two new works on the evolutionary modeling of the emission spectrum for the ionized gas that surrounds a young star cluster as a function of the gas metallicity and the cluster age and mass (Levesque et al. 2009; Martín-Manjón et al. 2009). In both works, the emission spectrum of HII regions is modeled for starburst galaxies and the results of the computations are particularly interesting for our case of a low gas metallicity in IC 10.

The parameters needed to compare the results of our observations with the mentioned model calculations are primarily the gas density and metallicity in the galaxy’s HII regions.

Estimating the Density of the Gaseous Medium

We found the electron density in the investigated nebulae of IC 10 from the [SII] doublet line intensity ratio from our MPFS observations to be within the range $N_e \simeq 20 - 250 \text{ cm}^{-3}$. In particular, the density reaches $N_e \simeq 60 - 100 \text{ cm}^{-3}$ in the nebula HL111c representing the brightest part of the shell HL111 and drops to $N_e \simeq 20 - 50 \text{ cm}^{-3}$ in the fainter regions of HL111. The results are presented below in Table 5, which gives

the nebular-averaged densities obtained from our MPFS and long-slit spectroscopic observations.

Estimating the Metallicity of the Gaseous Medium

The oxygen abundance in individual HII regions of IC 10 found in Lozinskaya et al. (2009) from long-slit spectroscopy lies within the range $12 + \log(\text{O}/\text{H}) = 7.59 - 8.52$; the mean metallicity of the gaseous medium in the galaxy is $12 + \log(\text{O}/\text{H}) \simeq 8.17 \pm 0.35$ or $Z = (0.18 \pm 0.14)Z_{\odot}$. The oxygen abundance variations in HII regions of IC 10 turned out to be large; we showed that they are attributable not only to the measurement errors of the line intensities but also to the real differences in the galaxy’s bright and faint ionized-gas regions.

The new results of our MPFS observations allow the data from Lozinskaya et al. (2009) to be supplemented. It also seems interesting to use a different metallicity estimation technique proposed by Pettini and Pagel (2004) both to interpret our MPFS observations and to refine our long-slit spectroscopic data.

The oxygen abundance was estimated in Lozinskaya et al (2009) from the relations found by Pilyugin and Thuan (2005) using the calibration dependence of $12 + \log(\text{O}/\text{H})$ on the relative intensities of strong [OII] and [OIII] lines. To estimate the abundances of oxygen and nitrogen and sulfur ions, we also used Eqs. (6) and (8) from Iso

to et al. (2006).

Yet another estimate of the oxygen abundance in HII regions can be obtained by the method proposed by Pettini and Pagel (2004) using the interstellar-extinction-independent ratio of the relative line intensities

$$\frac{I([\text{OIII}]\lambda 5007)/I(\text{H}\beta)}{I([\text{NII}]\lambda 6584)/I(\text{H}\alpha)}.$$

According to this paper, the oxygen abundance is defined by the relation

$$12 + \log(\text{O}/\text{H}) = 8.73 - 0.32 \times \text{O3N2},$$

where

$$\text{O3N2} = \log \frac{I([\text{OIII}]\lambda 5007)}{I(\text{H}\beta)} - \log \frac{I([\text{NII}]\lambda 6584)}{I(\text{H}\alpha)}$$

. In this case, the oxygen abundance is reliably estimated at $\text{O3N2} < 1.9$. Note that Bresolin et al. (2004) also confirmed that this relation works well in the range $12 + \log(\text{O}/\text{H}) < 8.4$.

Based on our MPFS observations, we estimated here the oxygen abundance $12 + \log(\text{O}/\text{H})$ by the above method for the individual nebulae HL111c, HL111d, and HL111e that form the shell structure of HL111 around the M24 group of WR stars, for the two HII regions HL111a and HL100 around the Wolf–Rayet WC4 star M12, and for the neighborhoods of the stars R10 (HL106 and HL106a), R12 (HL97, HL98), and M2 (HL4, HL6). The results are presented in Table 4. Its columns give: (1)— name of the HII region; (2)— O3N2 parameter; (3), (4), and (5) — derived relative O, N⁺, and S⁺ abundances, respectively. As follows from the table, the oxygen abundance $12 + \log(\text{O}/\text{H})$ for all nebulae varies within the range from 8.15 to 8.43. The minimum value corresponds to the center of current star formation in the vicinity of M24, with the exception of the southwestern fragment HL111e, where it is slightly higher. In the remaining HII regions investigated with the MPFS, the oxygen abundance is slightly higher and, on average, is close to 8.3.

We used the same method by Pettini and Pagel (2004) to reestimate the oxygen abundance in HII regions based on our long-slit spectroscopy. The results are also presented in Table 4. Comparison with the results from Lozinskaya et al. (2009)

shows that this method allows the scatter of oxygen abundance estimates to be reduced considerably compared to the method based on strong [OII] and [OIII] lines that we used previously.

To estimate the N⁺ and S⁺ abundances, we, as in Lozinskaya et al. (2009), used Eqs. (6) and (8) from Isotov et al. (2006), which include the extinction-dependent relative intensities $I([\text{NII}]\lambda 6548 + 6584\text{\AA})/I(\text{H}\beta)$ and $I([\text{SII}]\lambda 6717 + 6731\text{\AA})/I(\text{H}\beta)$. Therefore, we slightly modified their reduction technique to eliminate the possible errors related to the uncertainty in the correction for interstellar extinction during long-slit spectroscopic observations (the blue and red regions for spectrograms PA0, PA132, and PA268 were observed on different nights). In contrast to Lozinskaya et al. (2009), we did not correct the observed ratios for the color excess in the corresponding region but took the “theoretical” ratio $I(\text{H}\alpha):I(\text{H}\beta) = 2.86 : 1.00$, which, according to Aller (1984), is valid for typical electron density in a star-forming region of 20–300 cm⁻³ and electron temperature of $\simeq 10\,000$ K. The relative abundances $12 + \log(\text{N}^+/\text{H})$ and $12 \log(\text{S}^+/\text{H})$ refined in this way are presented in the last two columns of Table 4.

During our MPFS observations, we took the entire spectrum with the same exposure time and no problems with the extinction estimation arose.

We emphasize that the possible errors in the correction for interstellar extinction do not affect the oxygen abundance estimated by the method of Pettini and Pagel (2004), which is derived from the relative intensities of “neighbouring” lines.

According to Pettini and Pagel (2004), the dispersion of the dependence of the oxygen abundance on the ratio of $I([\text{OIII}]\lambda 5007)/I(\text{H}\beta)$ to $I([\text{NII}]\lambda 6584)/I(\text{H}\alpha)$ is ± 0.25 dex. However, comparison of our estimates from the MPFS and long-slit spectra shows agreement with an accuracy of at least ± 0.05 dex. Therefore, the observed difference between the oxygen abundances in different HII regions of IC 10, about 0.1 dex, seems real to us.

The oxygen abundance variations in the interstellar medium of IC 10, up to several tenths of dex, were considered in detail by Magrini and Gonçalves (2009), who pointed out the region of the most constant oxygen abundance $12 +$

Table 4: Estimates of the O, N⁺, and S⁺ abundances from our MPFS and long-slit spectroscopic observations

Region	O3N2	12 + log(O/H)	12 + log(N ⁺ /H)	12 + lg(S ⁺ /H)
MPFS observations				
HL111c	1.79 ± 0.12	8.16 ± 0.04	6.51 ± 0.10	5.91 ± 0.13
HL111d	1.75 ± 0.12	8.17 ± 0.04	6.56 ± 0.11	6.02 ± 0.10
HL111e	1.56 ± 0.09	8.23 ± 0.03	6.67 ± 0.08	6.16 ± 0.13
HL100	0.95 ± 0.14	8.43 ± 0.04	7.21 ± 0.15	6.89 ± 0.17
HL111a	1.39 ± 0.18	8.29 ± 0.05	6.95 ± 0.10	6.50 ± 0.12
HL106	1.16 ± 0.18	8.36 ± 0.05	6.81 ± 0.33	6.43 ± 0.43
HL106a	1.32 ± 0.13	8.31 ± 0.03	6.61 ± 0.11	6.08 ± 0.14
HL97	1.46 ± 0.21	8.26 ± 0.06	6.93 ± 0.28	6.54 ± 0.31
HL98	1.19 ± 0.18	8.35 ± 0.05	7.17 ± 0.41	6.92 ± 0.42
HL4	1.33 ± 0.48	8.30 ± 0.16	7.28 ± 0.41	6.24 ± 0.22
HL6	1.71 ± 0.36	8.18 ± 0.12	7.51 ± 0.22	7.02 ± 0.12
Long-slit spectroscopy				
HL111a	1.24 ± 0.14	8.33 ± 0.04	6.73 ± 0.13	6.10 ± 0.03
HL111b	1.01 ± 0.02	8.41 ± 0.01	6.86 ± 0.02	6.09 ± 0.01
HL111c	1.71 ± 0.01	8.18 ± 0.01	6.45 ± 0.10	5.67 ± 0.09
HL111d	1.48 ± 0.01	8.26 ± 0.01	6.70 ± 0.01	5.95 ± 0.01
HL111e	1.38 ± 0.01	8.29 ± 0.01	6.69 ± 0.02	5.97 ± 0.01
HL106	1.44 ± 0.16	8.27 ± 0.05	6.65 ± 0.23	6.00 ± 0.07
SS	0.73 ± 0.28	8.50 ± 0.09	7.07 ± 0.26	6.61 ± 0.10
HL37	1.83 ± 0.37	8.15 ± 0.12	6.71 ± 0.34	5.86 ± 0.05
HL45	2.03 ± 0.02	8.08 ± 0.01	6.13 ± 0.10	5.74 ± 0.01
HL50	1.72 ± 0.25	8.18 ± 0.08	6.54 ± 0.39	5.81 ± 0.34
HL100	0.96 ± 0.06	8.42 ± 0.02	6.90 ± 0.06	6.28 ± 0.02
HL89	0.90 ± 0.12	8.44 ± 0.04	6.93 ± 0.03	6.29 ± 0.03
WR M10	0.96 ± 0.07	8.42 ± 0.02	7.02 ± 0.07	6.45 ± 0.03
HL67	1.05 ± 0.14	8.39 ± 0.04	6.94 ± 0.24	6.20 ± 0.07
HL41	1.10 ± 0.05	8.38 ± 0.02	6.95 ± 0.12	6.04 ± 0.04
HL36	1.64 ± 0.05	8.20 ± 0.02	6.70 ± 0.14	5.72 ± 0.04
HL22	1.08 ± 0.03	8.38 ± 0.01	6.91 ± 0.11	5.98 ± 0.03
HL46-48	0.87 ± 0.03	8.45 ± 0.01	7.00 ± 0.09	6.27 ± 0.04

$\lg(\text{O}/\text{H}) = 8.2$ at a galactocentric distance of 0.2–0.5 kpc.

Note that for four regions common to our measurements and that by Magrini and Gonçalves (2009), the results are in good agreement. The nebula HL45, where our oxygen abundance estimate is appreciably, by almost 0.3 dex, lower, constitutes an exception. The high neutral oxygen abundance in this region, which may not be adequately taken into account in the method of Pettini and Pagel (2004), is probably responsible for the discrepancy.

Below, we use the density and metallicity of the gaseous medium found to choose appropriate theoretical diagnostic models.

Comparing the Observations of IC 10 with Theoretical Photoionization Models

Previously (Lozinskaya et al. 2009), we have already noted that the diagnostic diagrams of relative line intensities constructed from our long-slit spectroscopy agree poorly with the photoionization models for the gas metallicity found in IC 10, $Z = 0.2Z_{\odot}$. In particular, these diagnostic diagrams turned out to be in agreement with the theoretical calculations by Dopita et al. (2006) only for a metallicity from $Z = 0.4Z_{\odot}$ to $Z = (1-2)Z_{\odot}$. The comparison with the results of Cid Fernandes et al. (2007) and Asari et al. (2007), who summarized the gas metallicity estimates for $\simeq 85\,000$ starburst galaxies, made in Lozinskaya et al. (2009) also suggests that the HII regions in IC 10 agree excellently with the observations of other galaxies, but only in the range of metallicities from $Z = 0.3Z_{\odot}$ to $Z = 0.6Z_{\odot}$. Given the systematic shift by 0.2 dex revealed by Asari et al. (2007) between their metallicity estimates and those of Pilyugin and Thuan (2005) and Izotov et al. (2006) for 177 “common” objects, the lower limit of the range within which the nebulae of IC 10 investigated in Lozinskaya et al. (2009) fell is $Z = 0.2Z_{\odot}$. Comparison of our constructed diagnostic diagrams with the models by Charlton and Longhetti (2001) also showed that the HII regions of IC 10 fell within the metallicity range $Z = (0.2-1)Z_{\odot}$ (Lozinskaya et al. 2009).

The technique of theoretical diagnostic curves by Dopita et al. (2006) was improved in the new paper by Levesque et al. (2009), who modeled

the emission spectrum of HII regions for low-metallicity starburst galaxies. These authors used the Starburst99 evolutionary synthesis code and the Mappings III photoionization code (see Binette et al. 1985; Sutherland and Dopita 1993) modified by Groves et al. (2004), in which the influence of dust on the gas ionization was thoroughly taken into account. The spectral energy distributions for hot stars were taken according to the non-LTE models by Pauldrach et al. (2001) and Hillier and Miller (1998) with allowance made for the stellar wind and metal opacity. Levesque et al. (2009) considered the models of both a starburst and continuous star formation in a medium with a metallicity from $z = 0.001$ to $z = 0.04$ and with a density $n(\text{H}) = 100 \text{ cm}^{-3}$. The mass loss by O stars was taken in the form $dm/dt \simeq Z^{1/2}$; no correction for the metallicity effect was applied for WR stars (in contrast to Martín-Manjón et al. 2009; see below).

In Figs. 3a and 3b, the results of our MPFS and long-slit spectroscopic observations of HII regions and the observational data for IC 10 from Magrini and Gonçalves (2009) are compared with the diagnostic diagrams of relative line intensities, which are traditionally used to compare observations with ionization models, computed by Levesque et al. (2009). The calculations of $I([\text{OIII}]\lambda 5007\text{\AA})/I(\text{H}\beta)$ vs. $I([\text{NII}]\lambda 6584\text{\AA})/I(\text{H}\alpha)$ and $I([\text{SII}]\lambda 6717 + 6731\text{\AA})/I(\text{H}\alpha)$ vs. $I([\text{OIII}]\lambda 5007\text{\AA})/I(\text{H}\beta)$ are shown for a starburst at three gas metallicities and two ages: $t = 3 \text{ Myr}$ and $t = 5 \text{ Myr}$. The mean metallicity of IC 10 found above ($Z = 0.2Z_{\odot}$) corresponds to $z = 0.004$; below, we will estimate the age adopted for our comparison based on the models by Martín-Manjón et al. (2009).

As we see, the observations of nebulae in IC 10 agree poorly with the model calculations by Levesque et al. (2009) for the metallicity $Z = 0.2Z_{\odot}$ found here from our MPFS and long-slit spectroscopic observations and in Magrini and Gonçalves (2009).

Martín-Manjón et al. (2009) used new evolutionary stellar models (PopStar) from Mollá et al. (2009). In contrast to many other previously published models, these authors took the spectral energy distributions for O, B, and WR stars from Smith et al. (2002), who computed non-LTE models by taking into account the stellar wind and

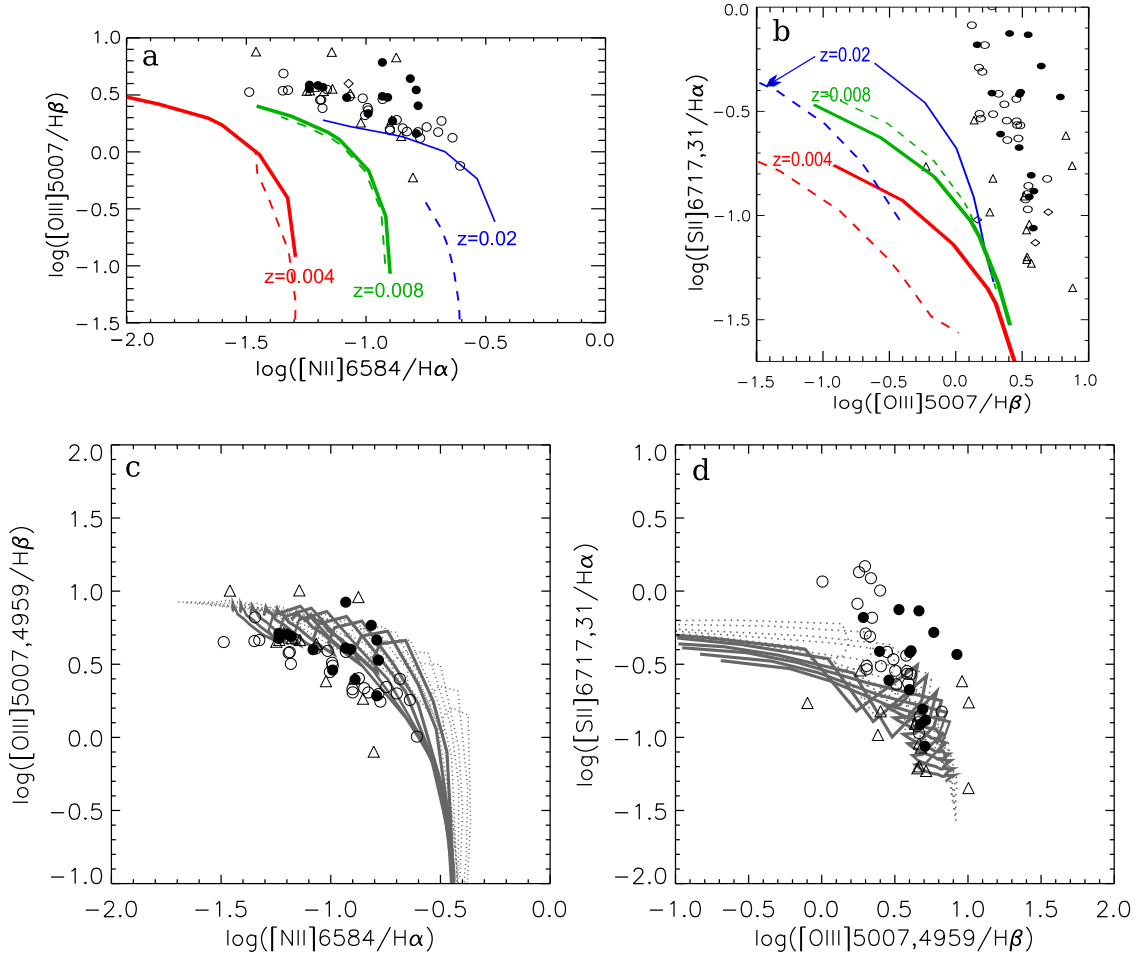


Fig. 3.— Comparison of the observations of HII regions in IC 10 with model calculations. The filled circles, open circles, and triangles indicate the results of our MPFS observations, our long-slit spectroscopy, and the data from Magrini and Gonçalves (2009), respectively. Panels (a) and (b) show the $I([\text{OIII}]\lambda 5007\text{\AA})/I(\text{H}\beta)$ vs. $I([\text{NII}]\lambda 6584\text{\AA})/I(\text{H}\alpha)$ and $I([\text{SII}]\lambda 6717 + 6731\text{\AA})/I(\text{H}\alpha)$ vs. $I([\text{OIII}]\lambda 5007\text{\AA})/I(\text{H}\beta)$ diagnostic diagrams computed by Levesque et al. (2009) for a starburst and two ages, 3 Myr (solid curves) and 5 Myr (dashed curves). The computations are given for three different gas metallicities (shown near the corresponding curves); $z = 0.004$ corresponds to the metallicity of HII regions in IC 10. Panels (c) and (d) show the families of $I([\text{OIII}]\lambda 4959 + 5007\text{\AA})/I(\text{H}\beta)$ vs. $I([\text{NII}]\lambda 6584\text{\AA})/I(\text{H}\alpha)$ and $I([\text{SII}]\lambda 6717 + 6731\text{\AA})/I(\text{H}\alpha)$ vs. $I([\text{OIII}]\lambda 4959 + 5007\text{\AA})/I(\text{H}\beta)$ diagnostic diagrams constructed by Martín-Manjón et al. (2009) for $z = 0.004$. Different curves correspond to different ionizing-cluster masses within the range $(0.12\text{--}2) \times 10^5 M_{\odot}$ (the lowest and highest masses are on the right and the left, respectively). The solid and dashed lines indicate the curves for $N_e \simeq 10\text{ cm}^{-3}$ and $N_e \simeq 100\text{ cm}^{-3}$, respectively.

blanketing in a revised scale of effective temperatures of O stars and, which is particularly important, temperatures of WR stars. The emission line intensities in HII regions were computed using the CLOUDY photoionization code (Ferland et al. 1998), with the decrease in the abundances

of Na, Al, Si, Ca, Fe, and Ni due to the presence of dust in the ionized region having been taken into account. The emission spectrum of an HII region during a starburst was computed by Martín-Manjón et al. (2009) for seven star cluster masses from $0.12 \times 10^5 M_{\odot}$ to $2.0 \times 10^5 M_{\odot}$, for

two densities of the interstellar medium, 10 and 100 cm^{-3} , in the range of cluster ages from 0.1 to 5.2 Myr, and for five gas metallicities in the range from $z = 0.001$ to $z = 0.04$.

Figures 3c and 3d show the $I([\text{OIII}]\lambda 4959 + 5007\text{\AA})/I(\text{H}\beta)$ vs. $I([\text{NII}]\lambda 6584\text{\AA})/I(\text{H}\alpha)$ and $I([\text{SII}]\lambda 6717 + 6731\text{\AA})/I(\text{H}\alpha)$ vs. $I([\text{OIII}]\lambda 4959 + 5007\text{\AA})/I(\text{H}\beta)$ diagnostic diagrams constructed by Martín-Manjón et al. (2009) for $z = 0.004$. Different curves correspond to the computations for different ionizing-cluster masses within the range $(0.12\text{--}2) \times 10^5 M_\odot$ (the lowest and highest masses are on the right and the left, respectively). The solid and dashed lines indicate the curves for densities $N_e \simeq 10 \text{ cm}^{-3}$ and $N_e \simeq 100 \text{ cm}^{-3}$, respectively. Different symbols in the figure indicate the mentioned relative line intensities averaged over the individual HII regions of IC 10 that we found from our MPFS and long-slit spectroscopic observations and the estimates from Magrini and Gonçalves (2009).

As we see, the observations generally agree with the theoretical dependences for a density within the range $N_e \simeq 10\text{--}100 \text{ cm}^{-3}$. Several points in the $I([\text{SII}]\lambda 6717 + 6731\text{\AA})/I(\text{H}\alpha)$ vs. $I([\text{OIII}]\lambda 4959 + 5007\text{\AA})/I(\text{H}\beta)$ diagram deviate from the theoretical dependence for a photoionized HII region toward higher sulfur line intensities. These points correspond to the long-slit spectrograms passing over the synchrotron superbubble and over several faint regions. The enhanced [SII] line intensity here may be related to the gas emission behind the shock front. Indeed, according to Lozinskaya and Moiseev (2007), the synchrotron superbubble is the remnant of a hypernova explosion.

In the regions HL67, HL89, HL97, HL98, HL100 and near the WR star M10, where an enhanced relative [SII] line intensity is also observed, we searched for high-velocity gas motions that would be indicative of the action of shock waves. For this purpose, we used our previous observations at the 6-m SAO telescope with the SCORPIO instrument and a scanning Fabry–Perot interferometer (FPI) in the $\text{H}\alpha$ and [SII] $\lambda 6717\text{\AA}$ lines, whose results are discussed in detail in Egorov et al. (2010).

The results of our search are presented in Fig. 4. Figure 4a shows the localization of the regions mentioned above, where an enhanced relative in-

tensity of the [SII] $\lambda 6717 + 6731\text{\AA}$ lines is observed. The $\text{H}\alpha$ and [SII] $\lambda 6717\text{\AA}$ line profiles in these regions constructed from our FPI observations are presented in Fig. 4b. As follows from the figure, in all regions of an enhanced relative sulfur line intensity, weak features are actually noticeable in the red and blue line wings at velocities from 70 to 160 km s^{-1} relative to the velocity of the peak. In the [SII] $\lambda 6717\text{\AA}$ line, prominent features in the wings are identified at the same velocities as those in $\text{H}\alpha$; the close coincidence of the velocities in the two lines is a strong argument for the reality of the weak features.

The detected high-velocity motions suggest the action of shock waves, which can be responsible for the observed enhanced relative intensity of the [SII] lines.

Thus, we made sure that the results of our observations agree well with the model calculations by Martín-Manjón et al. (2009). Therefore, below we use the theoretical calculations from this paper to analyze the observational data.

Modeling the emission spectra of HII regions allows such ionizing-cluster parameters as the age and mass as well as the ionization parameter to be estimated. For this purpose, we constructed the corresponding computed dependences using the data from Table 2b in the electronic version of the paper by Martín-Manjón et al. (2009). We constructed all of the computed dependences for the mean electron density $N_e = 100 \text{ cm}^{-3}$ and metallicity $z = 0.004$ found above. The results are presented in Figs. 5 and 6.

To estimate the ages of the most reliably identified ionization sources in several HII regions, we used the computed age dependences of the line intensities $I([\text{OIII}]\lambda 5007\text{\AA})/I(\text{H}\beta)$ (Fig. 5a), $I([\text{SII}]\lambda 6717\text{\AA})/I(\text{H}\alpha)$ (Fig. 5b), and $I([\text{NII}]\lambda 6584\text{\AA})/I(\text{H}\alpha)$ (Fig. 5c). As a parameter for the construction of each curve, we used the mass of the ionizing star cluster, which changes from one curve to another in the range from 0.12×10^5 to $2 \times 10^5 M_\odot$.

As follows from the figure, all of the clusters considered — T54 (in the HII shell HL111), T32 (ionizing HL50), T52 (ionizing the region around the star M12), T34?, T24 and T27 (ionizing the regions HL46 and HL48), T47 and poor T43? (ionizing HL89), and T50 and T53 (probable ionization

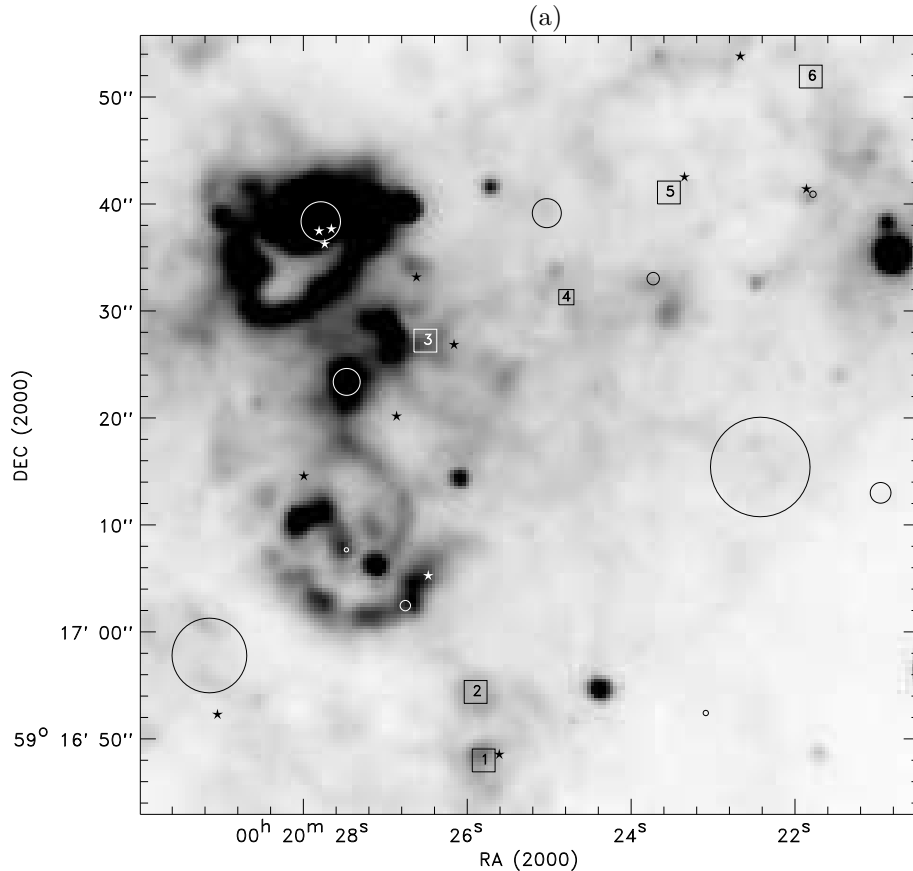


Fig. 4.— (a) The numbered squares indicate the localization of the regions where an enhanced intensity $I([\text{SII}]\lambda 6717 + 6731\text{\AA})/I(\text{H}\alpha)$ compared to the photoionization curves was revealed in Fig. 3; (b) examples of the $\text{H}\alpha$ (upper) and $[\text{SII}]\lambda 6717\text{\AA}$ (lower) line profiles from our FPI observations (in arbitrary units). The observed profile and the high-velocity components identified as an excess above the Voigt wings are shown. The region numbers indicated at the top correspond to the numbers of the squares in panel (a) (as in Fig. 1, the circles and asterisks represent the star clusters and WR stars).

sources of HL106) — have ages within the range from 2.5 to 5 Myr (in what follows, the sign “?” in Table 5 marks the clusters that are possible ionization sources of the corresponding HII region.) The clusters ionizing the shell HL111 and the region HL50 are youngest.

The use of three cluster age indicators based on different spectral lines in Fig. 5 shows certain discrepancies between them and, often, ambiguity. The difficulty of our estimations is compounded by the fact that all dependences are two-parameter ones (on cluster age and mass). Therefore, in determining the age, we chose the ranges of “intersection” of our estimates according to three crite-

ria, giving preference to the estimate based on the oxygen lines.

As an example, we will specify the corresponding parameters for the shell HL111. Judging by Fig. 5, the ages and masses of the clusters ionizing it lie within the following ranges:

- from the $[\text{OIII}]\lambda 5007/\text{H}\beta$ ratio:
 $t = 2.1\text{--}2.9$ Myr or $t = 3.6\text{--}4.1$ Myr,
 $M > 1.0 \times 10^5 M_{\odot}$;
- from the $[\text{SII}]\lambda 6717/\text{H}\alpha$ ratio:
 $t = 1.3\text{--}3.6$ Myr,
 $M = (0.12\text{--}2) \times 10^5 M_{\odot}$;

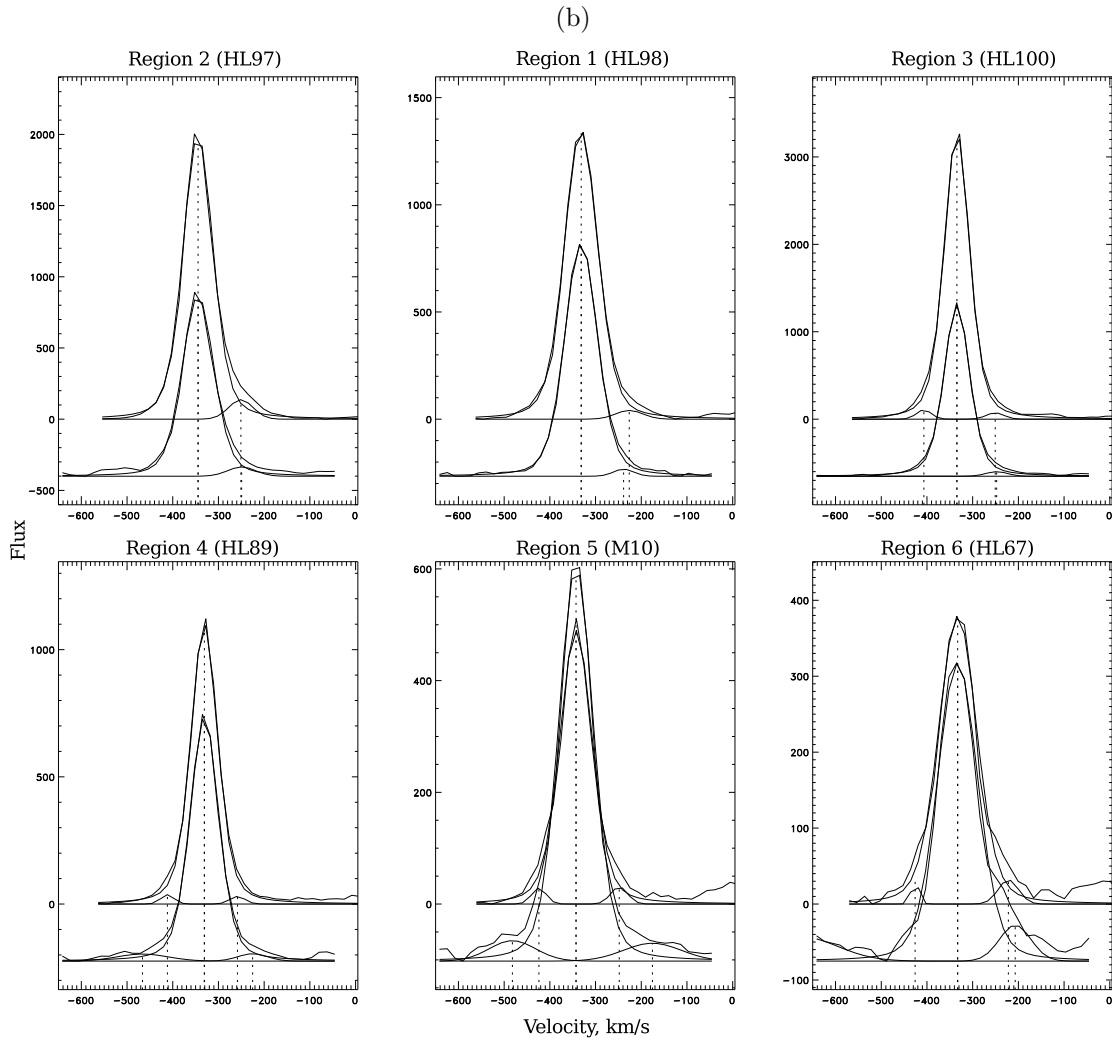


Fig. 4.— (Contd.)

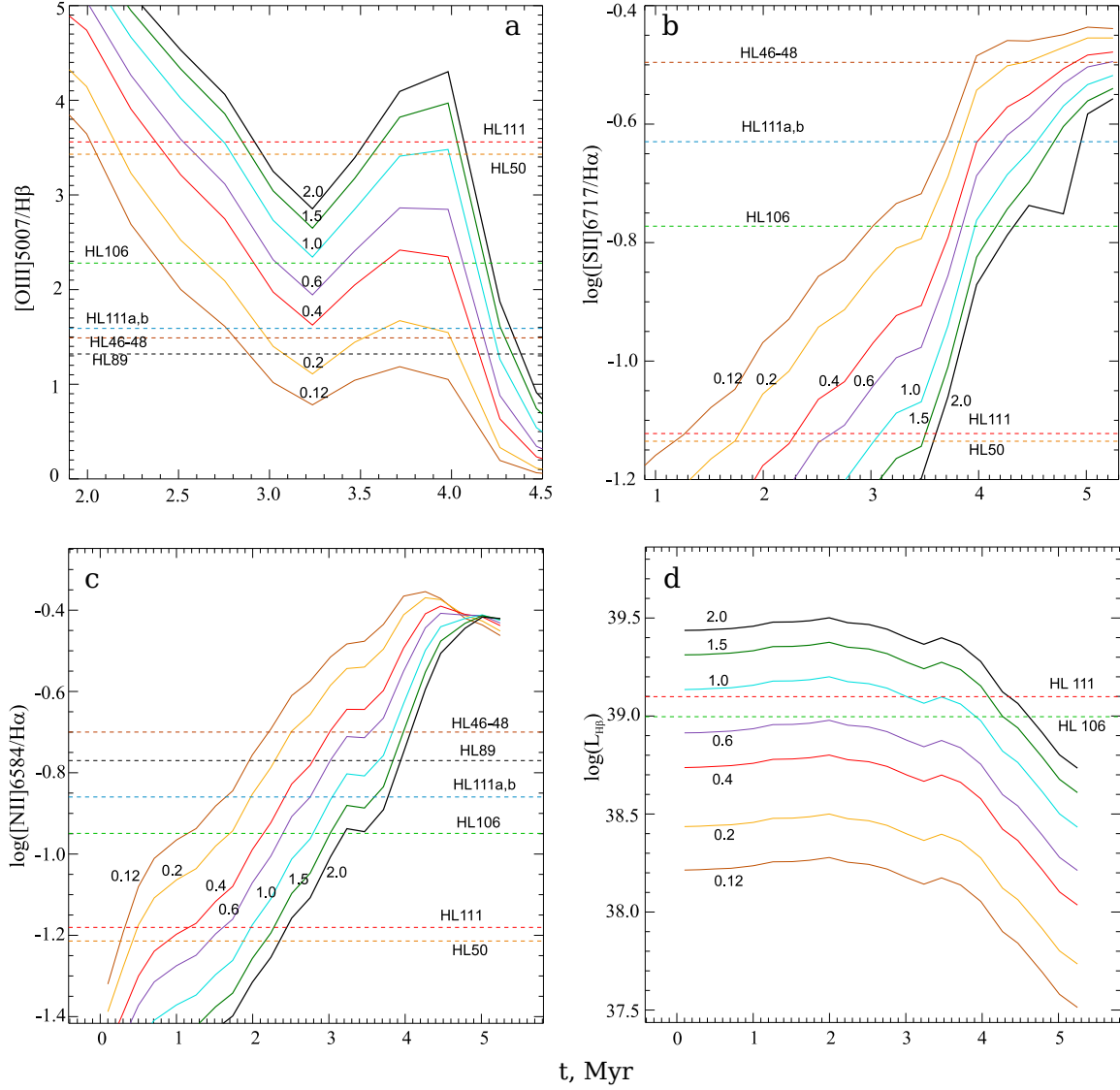


Fig. 5.— Computed dependences that we constructed from the data of Table 2b presented in the electronic version of the paper by Martín-Manjón et al. (2009) for the electron density $N_e = 100 \text{ cm}^{-3}$ and metallicity $z = 0.004$: the age dependences of the line intensities (a) $I([\text{OIII}]\lambda 5007\text{\AA})/I(\text{H}\beta)$, (b) $I([\text{SII}]\lambda 6717\text{\AA})/I(\text{H}\alpha)$, and (c) $I([\text{NII}]\lambda 6584\text{\AA})/I(\text{H}\alpha)$; (d) comparison of the observed luminosity $L(\text{H}\beta)$ for two HII regions, HL111 and HL106, with the computations by Martín-Manjón et al. (2009). The corresponding masses of the ionizing clusters are indicated near the model curves.

- from the $[\text{NII}]6584/\text{H}\alpha$ ratio:
 $t = 0.3\text{--}2.4$ Myr,
 $M = (0.12\text{--}2) \times 10^5 M_{\odot}$;

- from the luminosity $L(\text{H}\beta)$:
 $t = 3.0\text{--}4.3$ Myr,
 $M = (1.0\text{--}2.0) \times 10^5 M_{\odot}$ (see below).

Our estimate from the relative line intensity $[\text{NII}] 6584/\text{H}\alpha$ is least reliable, because the nitrogen lines in the nebula HL111 are weak, see Table 3.

Given these discrepancies, we can actually estimate the age only with an accuracy of ± 2 Myr. The scatter of cluster age estimates may be partly attributable to slight differences in metallicity and density of the HII regions associated with them (we neglected the possible slight differences when estimating the age).

However, the choice of an age from its possible options is facilitated considerably when Wolf-Rayet stars are presented in HII regions. This allows the lower age limit to be determined. Indeed, at $z = 0.004$, according to the evolutionary synthesis models by Mollá et al. (2009) used as a basis by Martín-Manjón et al. (2009), the stage at which the first Wolf-Rayet nitrogen-sequence (WN) stars appear corresponds to an age of about 3.2 Myr; the carbon-sequence (WC) stars emerge 1 Myr later. Since the components of the object M24 in the region HL111c probably belong to the nitrogen sequence of Wolf-Rayet stars (Vacca et al. 2007), we can exclude the ionizing-cluster age younger than 3 Myr.

Since the WC7-type star R10 is localized near the part of the region HL106 we observed, we can assign an age older than 4 Myr but no greater than 5 Myr to the ionizing cluster if we rely on the evolutionary synthesis models of the stellar population from Mollá et al. (2009).

Note also that we find the cluster age “at the time of ionization” from the spectra of HII regions. The ionization equilibrium time in an evolving HII region depends on the metallicity and density of the medium. According to Martín-Manjón et al. (2009), it is about 0.2 Myr at $z = 0.004$ and $N_e = 10 \text{ cm}^{-3}$ and decreases with increasing density. Thus, at $z \geq 0.004$ and the gas density in IC 10 found above, this time is considerably (by an order of magnitude!) smaller than the cluster

age. Therefore, the ages of the ionizing cluster and the ionized HII region are almost equal in our case.

Following the recommendations by Martín-Manjón et al. (2009) regarding the technique and sequence of parameter determination, we estimated the ages of the ionizing clusters from the relative line intensities $[\text{OIII}]/\text{H}\beta$, $[\text{SII}]/\text{H}\alpha$, and $[\text{NII}]/\text{H}\alpha$ in the spectra of the surrounding HII regions. In doing so, we used WR stars to refine the lower age limit. The cluster mass can then be found using the computed $\text{H}\beta$ luminosities of the HII region as a function of the age for clusters of different masses by comparing them with the observed luminosities in hydrogen lines. When estimating the $\text{H}\beta$ luminosity, we performed integration over the area of the corresponding HII region in the MPFS field. The results are shown in Fig. 5. We constructed different curves in the figure from the data of Table 2b in the electronic version of the paper by Martín-Manjón et al. (2009) for clusters of different masses. The horizontal lines indicate the luminosities of two nebulae found from our MPFS observations and corrected for extinction: HL111 around the cluster T54, which includes M24 (Hunter 4-1 and 4-2), and HL106, which is most likely ionized by the clusters T50 and T53.

We integrated the $\text{H}\beta$ emission from the shell HL111 to estimate its luminosity $L(\text{H}\beta) \simeq 1.3 \times 10^{39} \text{ erg s}^{-1}$ almost over the entire nebula covered by the MPFS field, with the exception of its small area on the east. The age of the cluster T54, about 3-4 Myr, can be reliably estimated both from the relative line intensities mentioned above and from the color indices of stars in Hunter (2001) and Vacca et al. (2007). Accordingly, we find the mass of the cluster T54 to be $M \simeq 1.0 \times 10^5 M_{\odot}$.

The mass estimate for the clusters ionizing HL106 is less reliable. First, only half of the nebula falls within the MPFS field and the luminosity $L(\text{H}\beta) = 1.0 \times 10^{39} \text{ erg s}^{-1}$ found has a low accuracy. Second, the age estimates from the relative line intensities $I([\text{OIII}]/\text{H}\beta)$ and $I([\text{NII}]/\text{H}\alpha)$ (about 4 Myr) and in Hunter (2001) (20-30 Myr) disagree significantly. Besides, we showed previously (Egorov et al. 2010) that the nebula HL106 could be an ionized shell surrounding a dense CO cloud. Therefore, the mass estimate for the

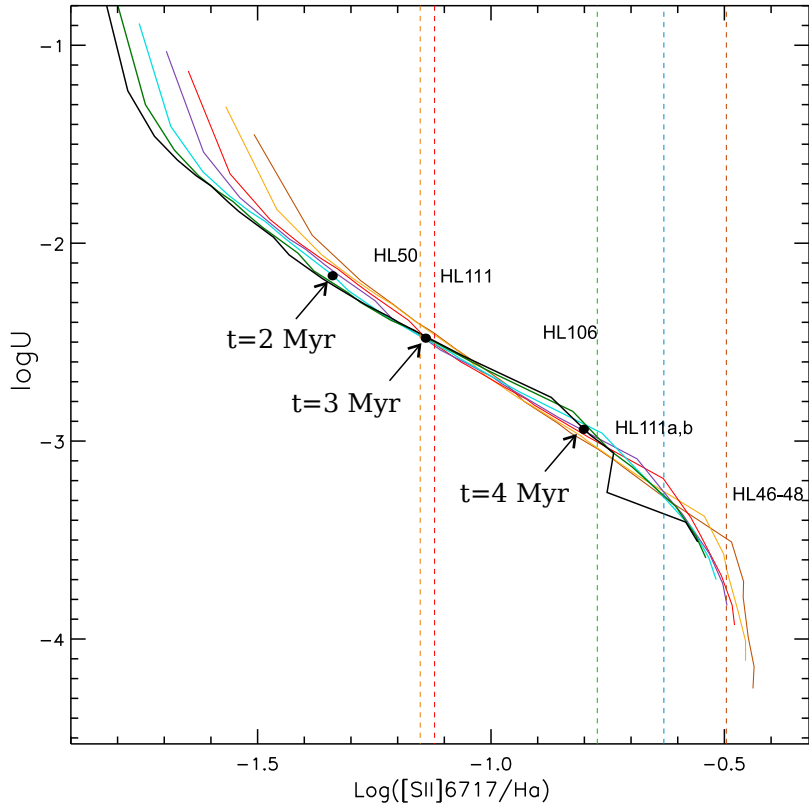


Fig. 6.— Relations between the line intensity ratio $I([\text{SII}]\lambda 6717\text{\AA})/I(\text{H}\alpha)$ and ionization parameter U constructed from the data of Table 2b in the electronic version of the paper by Martín-Manjón et al. (2009) for the metallicity $z = 0.004$ and density $N_e = 100 \text{ cm}^{-3}$. The cluster age changes along the curves from the upper left corner to the lower right one. The dashed vertical lines indicate the observed relative intensities corresponding to the HII regions.

clusters T50 and T53, $M \simeq 0.5 \times 10^5 M_\odot$, is only approximate.

When estimating the cluster masses, we also took into account the positions of the HII regions in Fig. 5, where each curve corresponds to an age of the ionizing star cluster in the range from 0.12×10^5 to $2 \times 10^5 M_\odot$.

The computations by Martín-Manjón et al. (2009) also allow the ionization parameter (U) to be estimated from the relative line intensity $I([\text{SII}]\lambda 6717\text{\AA})/I(\text{H}\alpha)$. Figure 6 shows the relations between the relative line intensity $I([\text{SII}]\lambda 6717\text{\AA})/I(\text{H}\alpha)$ and parameter U that we constructed from the data of Table 2b in the electronic version of the above paper for the gas metallicity in this galaxy $z = 0.004$ and density $N_e = 100 \text{ cm}^{-3}$. As we see, the relation between these parameters is virtually independent of the cluster mass. The age in Fig. 6 rises along the merging curves from the upper left corner to the lower right one. The vertical lines indicate the values of $I([\text{SII}]\lambda 6717\text{\AA})/I(\text{H}\alpha)$ that we found in the investigated HII regions.

For the arc HL111c near M24, Vacca et al. (2007) found the flux of ionizing radiation with a wavelength shorter than 912 \AA to be $Q(\text{H}) = (3-6) \times 10^{50} \text{ phot. s}^{-1}$. Our estimate of the photon luminosity for the entire shell HL111 (HL111c+HL111d+HL111e) from the observed $\text{H}\beta$ flux corrected for interstellar extinction is $Q(\text{H}) \geq 3.2 \times 10^{51} \text{ phot. s}^{-1}$.

For a cluster age of 3–4 Myr, Mollá et al. (2009) give the ratio of the photon luminosity of the ionizing stars to the cluster mass $\log(Q(\text{H})/M) = 46.75$ at $z = 0.004$. If the cluster mass in HL111 is taken to be $M \simeq 10^5 M_\odot$, then we find $Q(\text{H}) = 5.6 \times 10^{51} \text{ phot. s}^{-1}$. Thus, the estimates of the flux of ionizing radiation obtained from the observations and model calculations are in good agreement.

Table 5 presents all of the parameters of the clusters ionizing the most thoroughly studied HII regions obtained in this paper. Its respective columns give: (1)— name of the nebula, (2)— ionizing cluster according to the list by Tikhonov and Galazutdinova (2010) (the sign “?” marks the clusters whose contribution is also possible), (3)— gas density in the nebula, (4)— line luminosity $L(\text{H}\beta)$, (5)— cluster age, (6)— cluster mass, (7)—

ionization parameter.

Summarizing the results of our analysis of the gas emission spectrum and ionization sources in IC 10 based on our long-slit and MPFS observations at the 6-m SAO telescope, we conclude the following.

Our new estimates of the gas metallicity in the galaxy from both series of observations using the technique by Pettini and Pagel (2004) different from that in Lozinskaya et al. (2009) allowed the scatter of values for different nebulae to be reduced considerably, but they did not change the galaxy-averaged value of $Z = 0.2Z_\odot$ that we found previously. The new estimates of the relative abundances of oxygen and nitrogen and sulfur ions in nebulae from our MPFS observations and refined estimates from long-slit spectrograms are gathered in Table 4.

In Lozinskaya et al. (2009), we showed that the results of our observations of HII regions in IC 10 agree poorly with the previously published model calculations for photoionized nebulae for the metallicity found. Comparison with the new improved ionization models by Levesque et al. (2009) showed that the observed $I([\text{OIII}]\lambda 5007\text{\AA})/I(\text{H}\beta)$ vs. $I([\text{NII}]\lambda 6584\text{\AA})/I(\text{H}\alpha)$ and vs. $I([\text{SII}]\lambda 6717 + 6731\text{\AA})/I(\text{H}\alpha)$ diagnostic diagrams agree poorly with the computations for the gas metallicity in the galaxy that we and Magrini and Gonçalves (2009) found.

At the same time, comparison of the observed diagnostic diagrams of relative line intensities with the new ionization models by Martín-Manjón et al. (2009) showed that the observations of IC 10 are in good agreement with these computations. The effect of an enhanced relative intensity $I([\text{SII}])/I(\text{H}\alpha)$ in several nebulae compared to the model photoionized HII region that is clearly seen in Fig. 3 may be attributable to the contribution from the gas emission behind the front of the shocks triggered by supernova explosions and stellar winds. Indeed, some of the “outlying” points correspond to the synchrotron superbubble — the remnant of a hypernova explosion (see Lozinskaya and Moiseev 2007). In other nebulae, where an enhancement of the relative intensity $I([\text{SII}])/I(\text{H}\alpha)$ is also observed, our FPI observations revealed weak features in the $\text{H}\alpha$ and $[\text{SII}]$ line profiles at supersonic velocities as high as 100–150 km s^{-1} relative to the velocity of the peak, which is in-

Table 5: Parameters of the HII regions and the clusters ionizing them

Region	Cluster	N_e , cm^{-3}	$L(\text{H}\beta)$, $10^{39} \text{ erg s}^{-1}$	Age, Myr	Mass, $10^5 M_\odot$	$\lg(U)$
HL111	T54	70	1.3	3.5–4.0	1.0–1.5	–2.5
HL106	T50, T53	200	1.0	4.0–4.5	≥ 1.0	–3.0
HL50	T32	30	–	3.4–3.6 or 2.5–3.0	1.5–2.0 or 0.4–1.0	–2.47
HL111a,b HL100	T52	200	–	3.8–4.5	0.2–0.6	–3.27
HL46-48	T34?, T24, T27	–	–	4.0–5.0	0.2–0.4	–3.6
HL89	T47, T43?	200	–	>3	≥ 0.2	–

dicative of the action of shock waves. A prominent action of shock waves in IC 10 is also suggested by the filamentary structure of the entire $\text{H}\alpha$ emission region in the galaxy.

Thus, we made sure that among the large number of published theoretical evolutionary models for the emission spectrum of HII regions during a starburst, our observations of the galaxy IC 10 are in best agreement with the computations by Martín-Manjón et al. (2009). Therefore, the presented results of our MPFS observations and our long-slit spectroscopic data are interpreted here in terms of the improved ionization models by these authors. Using these computations, we determined the ionization parameter and the ages and masses of the ionizing clusters from the spectra of several most thoroughly studied HII regions in the galaxy. When estimating the age, we also took into account the presence of nitrogen- and carbon-sequence WR stars, which gives its lower limit. The cluster ages and masses found in the investigated star-forming region of IC 10 lie within the range 2.5–5 Myr and in the range from 0.2×10^5 to $10^5 M_\odot$.

CONCLUSIONS

This paper continues the studies of the ionized gas emission spectrum in the Irr starburst galaxy IC 10 begun by Lozinskaya et al. (2009) based on long-slit spectroscopy. Here, we presented new results of our observations of selected galactic fields with the panoramic MPFS; we also used the results of our observations with a long-slit spectrograph and a scanning Fabry–Perot interferometer.

To estimate the gas metallicity in the galaxy, we used the method by Pettini and Pagel (2000) dif-

ferent from that used in Lozinskaya et al. (2009). The gas metallicity was determined by this method both from our new MPFS observations and from our long-slit spectroscopy. The metallicity estimated in this way is characterized by a smaller scatter of values for individual nebulae but it does not change the galaxy-averaged value.

Previously (Lozinskaya et al. 2009), we showed that the results of our observations of HII regions in IC 10 agree poorly with the published model calculations for photoionized nebulae at the metallicity $Z = 0.2Z_\odot$ found. In this paper, we made such a comparison with two new computed ionization models from Levesque et al. (2009) and Martín-Manjón et al. (2009).

We showed that the observations of IC 10 agree well with the computations by Martín-Manjón et al. (2009). We explained the noticeable (in several nebulae) effect of an enhanced relative intensity $I([\text{SII}])/I(\text{H}\alpha)$ compared to the model photoionized HII region by the contribution from the gas emission behind the fronts of the shocks triggered by supernova explosions and stellar winds. Indeed, some of the “outlying” points correspond to the synchrotron superbubble — the remnant of a hypernova explosion (Lozinskaya and Moiseev 2007); in other nebulae with an enhanced relative intensity $I([\text{SII}])/I(\text{H}\alpha)$, our FPI observation revealed weak features in the $\text{H}\alpha$ and $[\text{SII}]$ line profiles at supersonic speeds as high as 100–150 km s^{-1} , suggesting the action of shocks.

Having made sure that among the large number of published theoretical evolutionary models for the emission spectrum of HII regions in a starburst galaxy, our observations of IC 10 agree best with the computations by Martín-Manjón et al. (2009),

we used these computations to analyze our MPFS and long-slit spectroscopic observations. Based on the ionization models of these authors, we determined the ionization parameter and the ages and masses of the ionizing clusters from the spectra of several most thoroughly studied HII regions. In our estimations, we took also into account the presence of WR stars, which gives a lower limit for the age. The cluster ages found in the investigated star-forming region of IC 10 lie within the range 2.5–5 Myr, while the masses of the ionizing star clusters lie within the range from 0.2×10^5 to $10^5 M_{\odot}$.

After our paper was accepted for publication, a paper by López-Sánchez et al. (2010) appeared (ArXiv1010.1806) with the results of the most detailed spectral observations of the HL111 region with 3.5 m telescope at Calar Alto Observatory with a spatial resolution of $1''$. For the whole HL111 region these authors derived the temperature $T_e=10500$ K, the oxygen abundance $12+\lg(\text{O}/\text{H}) = 8.26 \pm 0.09$ and the age of the recent star-formation episode of about 3.3 Myr – all the data are in full agreement with our results. The only discrepancy in the fluxes of hydrogen lines in HL111 may be due to our not too reliable absolute calibration of $\text{H}\beta$ line. In two spaxels coinciding with WR star M24B these authors tentatively detected the broad HeII 4686 line produced by a single WNL star. At the same location a possible N/O and He/H medium enrichment was found expected for the pollution by the WR-ejecta.

ACKNOWLEDGMENTS

This work was supported by the Russian Foundation for Basic Research (project nos. 07-02-00227 and 10-02-00091). We thank N.A. Tikhonov, M.E. Sharina and O.A. Galazutdinova for their help in discussing the accuracy of the coordinates of star clusters. O.V. Egorov and A.V. Moiseev thank the hank the ‘Dynasty’ Fund for financial support. The work is based on the observational data obtained with the 6-m SAO telescope funded by the Ministry of Science of Russia (registration no. 01-43). When working on the paper, we used the NASA/IPAC Extragalactic Database (NED) operated by the Jet Propulsion Laboratory of the California Institute of Technology under contract with the National Aeronautics

and Space Administration (USA).

Translated by V. Astakhov

REFERENCES

1. V. L. Afanasiev, S. N. Dodonov, and A. V. Moiseev, *Stellar Dynamics: from Classic to Modern*, Ed. by L. P. Osipkov and I. I. Nikiforov (SPb. Univ., St.-Petersburg), p.103 (2001) .
2. V. L. Afanasiev and A. V. Moiseev, *Astron. Lett.* **31**, 194 (2005).
3. L. H. Aller, *Physics of Thermal Gaseous Nebulae* (Reidel, Dordrecht, 1984).
4. N. V. Asari, R. Cid Fernandes, G. Stasinska, et al., **381**, 263 (2007).
5. L. Binette, M. A. Dopita, and I. R. Tuohy, *Astrophys. J.* **297**, 476 (1985).
6. F. Bresolin, D. R. Garnett, and R. C. Kennicutt, Jr., *Astrophys. J.* **615**, 228 (2004).
7. A. Bullejos and M. Rozado, *Rev. Mex. (Ser. de Conf.)* **12**, 254 (2002).
8. S. Charlot and M. Longhetti, *Mon. Not. R. Astron. Soc.* **323**, 887 (2001).
9. K. T. Chyzy, J. Knapik, D. J. Bomans, et al., *Astron. Astrophys.* **405**, 513 (2003).
10. R. Cid Fernandes, N. V. Asari, L. Sodre, et al., *MNRAS* **375**, 16 (2007).
11. P. A. Crowther, L. Drissen, J. B. Abbott, et al., *Astron. Astrophys.* **404**, 483 (2003).
12. M. A. Dopita, J. Fischera, R. S. Sutherland, et al., *Astrophys. J. Suppl. Ser.* **167**, 177 (2006).
13. O. V. Egorov, T. A. Lozinskaya, and A. V. Moiseev, *Astron. Rep.* **54**, 277 (2010).
14. G. I. Ferland, K. T. Korista, D. A. Verner, et al., *Publ. Astron. Soc. Pacif.* **110**, 761 (1998).

15. A. Gil de Paz, B. F. Madore, and O. Pe-
vunova, *Astrophys. J. Suppl. Ser.* **147**, 29
(2003).
16. B. Groves, M. Dopita, and R. Sutherland,
Astroph. J. Suppl. Ser. **153**, 9 (2004).
17. D. J. Hillier and D. L. Miller, *Astrophys. J.*
496, 407 (1998).
18. P. Hodge and M. G. Lee, *Publ. Astron. Soc.*
Pacif. **102**, 26 (1990).
19. D. A. Hunter, *Astrophys. J.* **559**, 225
(2001).
20. Y. I. Izotov, G. Stasinska, G. Meynet, et al.,
Astron. Astrophys. **448**, 955 (2006).
21. A. Leroy, A. Bolatto, F. Walter, and L. Blitz,
Astrophys. J. **643**, 825 (2006).
22. E. M. Levesque, L. J. Kewley, and K. L. Lar-
son, *astro-ph/0908.0460* (2009).
23. A. R. López-Sánchez, A. Mesa-Delgado,
L. López-Martín and C. Esteban, *astro-
ph/1010.1806L* (2010)
24. T. A. Lozinskaya and A. V. Moiseev,
MNRAS **381**, 26L (2007).
25. T. A. Lozinskaya, A. V. Moiseev,
N. Yu. Podorvanyuk, and A. N. Burenkov,
Astron. Lett. **34**, 217 (2008).
26. T. A. Lozinskaya, O. V. Egorov, A. V. Moi-
seev, and D. V. Bizyaev, *Astron. Lett.* **35**,
730 (2009).
27. L. Magrini and D. R. Gonçalves, *MNRAS*
398, 280 (2009).
28. M. L. Martín-Manjón, M. L. García-Vargas,
M. Mollá, and A. I. Díaz, *MNRAS* **403**, 2012
(2010), *astro-ph/0912.4730* (2009).
29. P. Massey and S. Holmes, *Astrophys. J.*
580, L35 (2002).
30. P. Massey, T. E. Armandroff, and
P. S. Conti, *Astron. J.* **103**, 1159 (1992).
31. P. Massey, K. Olsen, P. Hodge, et al., *As-
tron. J.* **133**, 2393 (2007).
32. M. Mollá, M. L. García-Vargas, and A. Bres-
san, *MNRAS* **398**, 451 (2009).
33. A. W. A. Pauldrach, T. L. Hoffmann, and
M. Lennon, *Astron. Astrophys.* **375**, 161
(2001).
34. M. Pettini and B. E. J. Pagel, *Mon. Not.*
R. Astron. Soc. **348**, L59 (2004).
35. L. S. Pilyugin and T. X. Thuan, *Astrophys.*
J. **631**, 231 (2005).
36. M. G. Richer, A. Bullejos, J. Borissova, et
al., *Astron. Astrophys.* **370**, 34 (2001).
37. M. Rosado, M. Valdez-Gutierrez, A. Bulle-
jos, et al., *ASP Conf. Ser.* **282**, 50 (2002).
38. P. Royer, S. J. Smartt, J. Manfroid, and
J. Vreux, *Astron. Astrophys.* **366**, L1
(2001).
39. N. Sanna, G. Bono, P. B. Stetson, et al.,
Astrophys. J. **699**, L84 (2009).
40. M. E. Sharina, R. Chandar, T. H. Puzia, et
al., *MNRAS*, *astro-ph/1002.2144* (2009).
41. L. Smith, R. Norris, and P. Crowther,
MNRAS **337**, 1309 (2002).
42. R. Sutherland and M. A. Dopita, *Astrophys.*
J. **88**, 253 (1993).
43. J. C. Thurow and E. M. Wilcots, *Astron. J.*
129, 745 (2005).
44. N. A. Tikhonov, O. A. Galazutdinova, *As-
tron. Lett.* **35**, 748 (2009).
45. W. D. Vacca, C. D. Sheehy, and J. R. Gra-
ham, *Astrophys. J.* **662**, 272 (2007).
46. E. M. Wilcots and B. W. Miller, *Astron. J.*
116, 2363 (1998).
47. H. Yang and E. D. Skillman, *Astron. J.* **106**,
1448 (1993).
48. J. Yin, L. Magrini, F. Matteucci, et al.,
astro-ph/1005.3500 (2010).
49. D. B. Zucker, *Bull. Am. Astron. Soc.* **32**,
1456 (2000).
50. D. B. Zucker, *Bull. Am. Astron. Soc.* **34**,
1147 (2002).